Experimental determination of the magnetic interactions of frustrated Cairo pentagon lattice materials

Manh Duc Le [1,2,*] Elisa M. Wheeler [3,4] Jaehong Jeong,[2,5] K. Ramesh Kumar,[2] Seongsu Lee,[6] Chang-Hee Lee [6]
Myeong Jun Oh,[7] Youn-Jung Jo,[7] Akihiro Kondo,[8] Koichi Kindo,[8] U. Stuhr [9] B. Fåk,[3] M. Enderle,[3] Dmitry Batuk,[10]
Artem M. Abakumov,[11] Alexander A. Tsirlin,[12] and Je-Geun Park[2,5,13]

[1]*ISIS Neutron and Muon Source, Rutherford Appleton Laboratory, Chilton, Didcot OX11 0QX, United Kingdom*
[2]*IBS Research Center for Correlated Electron Systems, Seoul National University, Seoul 08826, Korea*
[3]*Institut Laue-Langevin, Avenue des Martyrs, CS 20156, F-38042 Grenoble Cédex 9, France*
[4]*Cellule DATA, Université de Strasbourg, 20a rue René Descartes, F-67000 Strasbourg, France*
[5]*Department of Physics and Astronomy, Seoul National University, Seoul 08826, Korea*
[6]*Neutron Science Division, Korea Atomic Energy Research Institute, Daejeon 34057, Korea*
[7]*Department of Physics, Kyungpook National University, Daegu 41566, Korea*
[8]*Institute for Solid State Physics, The University of Tokyo, Kashiwa, Chiba 277-8581, Japan*
[9]*Laboratory for Neutron Scattering, Paul-Scherrer-Institut, 5232 Villigen PSI, Switzerland*
[10]*EMAT, University of Antwerp, Groenenborgerlaan 171, B-2020 Antwerp, Belgium*
[11]*Skolkovo Institute of Science and Technology, Nobel Str. 3, 143026 Moscow, Russia*
[12]*Experimental Physics VI, Center for Electronic Correlations and Magnetism, University of Augsburg, 86159 Augsburg, Germany*
[13]*Center for Quantum Materials, Seoul National University, Seoul 08826, Korea*

We present inelastic neutron scattering measurements of the Cairo pentagon lattice magnets $Bi_2Fe_4O_9$ and $Bi_4Fe_5O_{13}F$, supported by high field magnetization measurements of $Bi_2Fe_4O_9$. Using linear spin wave theory and mean-field analyses we determine the spin exchange interactions and single-ion anisotropy in these materials. The Cairo lattice is geometrically frustrated and consists of two inequivalent magnetic sites, both occupied by Fe^{3+} ions and connected by two competing nearest neighbor interactions. We found that one of these interactions, coupling nearest neighbor spins on the threefold symmetric sites, is extremely strong and antiferromagnetic. These strongly coupled dimers are then weakly coupled to a framework formed from spins occupying the other inequivalent site. In addition, we found that the Fe^{3+} $S = 5/2$ spins have a non-negligible single-ion anisotropy, which manifests as a spin anisotropy gap in the neutron spectrum and a spin-flop transition in high field magnetization measurements.

I. INTRODUCTION

Competing exchange interactions in geometrically frustrated magnets may lead to a large number of degenerate ground states [1]. The prototypical case is the Ising antiferromagnet on a triangular lattice, in which only half of the nearest neighbor interactions may be satisfied by any particular spin arrangement. In the more conventional Heisenberg case, where the spins are free to adopt a range of orientations, a unique ground state with spins oriented at 120° to their neighbors may be stabilized. Besides triangles, other odd-vertex polygons will also exhibit geometrical frustration, however a tiling of these shapes in a regular crystal is forbidden by symmetry. Nonetheless, lattices exists which consists of tilings of irregular odd-vertex polygons, of which the Cairo pentagonal lattice is one. In this case, the pentagons have four equal and one unequal sides, as illustrated in Fig. 1(a).

This gives rise to two inequivalent sites with three- and fourfold rotational symmetry perpendicular to the pentagon

plane, which are connected by two competing nearest neighbor interactions. One coupling is along the four equal edges which links threefold to fourfold sites ($\mathcal{J}_{43}$), and the other goes via the single unequal edge of the pentagon, which links two threefold sites ($\mathcal{J}_{33}$). When these interactions are antiferromagnetic the system is geometrically frustrated and a frustration index may be constructed as $x = \mathcal{J}_{43}/\mathcal{J}_{33}$. This is small when $\mathcal{J}_{33}$ dominates, leading the nearest neighbor threefold sites (denoted Fe^3) to form antiparallel pairs which may be thought of as dimers. Neighboring threefold pairs are connected via the fourfold sites (denoted Fe^4) and the competing $\mathcal{J}_{43}$ interaction. If $\mathcal{J}_{43}$ is small, then for classical (Heisenberg) spins, a noncollinear spin configuration analogous to the 120° structure of the triangular lattice antiferromagnets is theoretically predicted [2]. In this *orthogonal* structure, shown in Fig. 1(b), neighboring threefold pairs are aligned at 90° to each other, as are next-nearest neighbor fourfold spins. For quantum spins, in the small x limit, instead of the orthogonal structure, a collinear, partial ordered structure is predicted to be stabilized, where half of the threefold sites do not order. Finally, when $\mathcal{J}_{43}$ dominates, at large x, a collinear ferrimagnetic structure is predicted where the threefold and
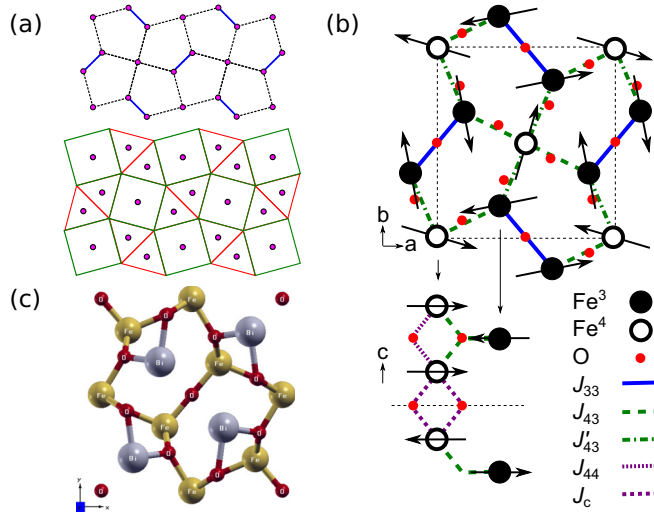
104423-1

FIG. 1. (a) The Cairo lattice, with magnetic ions at the vertices of a lattice of irregular pentagons. Alternatively, the magnetic ions may be visualized as being enclosed by an edge-shared network of squares and equilateral triangles. (b) Sketch of the crystal and magnetic structure of $Bi_2Fe_4O_9$ showing only Fe and O atoms and the Fe-O-Fe superexchange pathways. The Fe^3 sites are the same as threefold symmetric sites in the Cairo lattice, while pairs of Fe^4 spins occupy positions above and below the Cairo-lattice fourfold symmetric sites. (c) View of the crystal structure perpendicular to the c axis, with Bi atoms in gray, Fe in yellow, and O in red.

fourfold sublattices are each individually ferromagnetic but are anti-aligned with each other. In between these limits, when $x \approx \sqrt{2}$, Rousochatzakis *et al.* [2] predict that a spin nematic phase would be realized for quantum spin.

In the two experimental realizations of the Cairo lattice studied in this work, $Bi_2Fe_4O_9$ and $Bi_4Fe_5O_{13}F$, the $\mathcal{J}_{33}$ interaction is expected to dominate due to the 180° Fe-O-Fe bond angle which is favorable for large antiferromagnetic superexchange interactions. In contrast, the other nearest neighbor interactions have 120°–130° bond angles which also leads to antiferromagnetic couplings but are much weaker. Indeed the orthogonal structure is observed at low temperatures in both $Bi_2Fe_4O_9$ [3] and $Bi_4Fe_5O_{13}F$ [4,5]. This orthogonal structure (expected in the case of low frustration index x) is noncollinear like the triangular 120° structure, and may lead to interesting magnetic excitations, as was recently observed for the 120° system $(Y,Lu)MnO_3$ [6,7].

In order to verify the exchange interactions, and thus experimentally determine x, and to compare with the theoretical phase diagram of [2], we have measured the magnon spectrum of $Bi_2Fe_4O_9$, and the related material $Bi_4Fe_5O_{13}F$, which is formed by interleaving additional layers of Fe^{3+} ($S = 5/2$) spins (denoted Fe^{int}) in between the fourfold sites along c between the pentagonal layers.

II. METHODS

Inelastic neutron scattering measurements were performed on single crystals of $Bi_2Fe_4O_9$ on the triple-axis spectrometers EIGER (at the Paul-Scherrer-Institut, Switzerland) [8] and IN20 (at the Institut-Laue-Langevin, France) [9]. A co-aligned

array of six crystals was used for the EIGER measurements with total sample mass ≈ 0.6 g, while the IN20 measurements used only the largest crystal with mass 0.28 g. The crystals were grown in Bi_2O_3 flux in Pt crucibles, and their crystallinity and orientations were checked using the Bio-D diffractometer at HANARO, Korea [10]. The crystals were single phased and found to adopt the *Pbam* space group with lattice parameters $a = 7.99$ Å, $b = 8.43$ Å, and $c = 6.01$ Å, in agreement with the literature [3]. A small 15 mg single crystal was used for high field magnetization measurements at ISSP, Japan, in pulsed fields up to 65 T, with the crystals oriented with the field along [110] and [001] in turn.

In the EIGER measurements the crystals were mounted with $[hh0] - [00l]$ directions in the horizontal scattering plane, while on IN20 the $[h00] - [0k0]$ directions were horizontal. In the IN20 measurements, small out-of-plane momentum transfers were accessible by tilting the cryostat. Both spectrometers were operated with fixed final energy $E_F = 14.7$ meV in the W configuration (scattering sense -1, $+1$, -1 at the monochromator, sample, and analyzer, respectively) with open collimation (without collimators between the axes). We used the double-focusing Si(111) monochromator and PG(002) analyzer on IN20, while a focused PG(002) monochromator and analyzer set up was used on EIGER. Both setups used a PG filter before the analyzer. Because of the lower flux of EIGER, measurements there were carried out at 200 K, just below $T_N = 245$ K, where the larger magnon population factor enhances the signal. In addition to unpolarized measurements [11] of the magnon dispersion at 2 K on IN20, we also measured the XYZ polarization dependence at selected Brillouin zone center and zone edge positions. In this case, the horizontally focused Heusler monochromator and analyzer was used with a flipper on the scattered beam and a PG filter in front of the analyzer. Helmholtz coils were used to align the neutron polarization to be parallel to the momentum transfer (x), perpendicular to this in the horizontal scattering plane (y) and vertically (z).

Supplementary inelastic neutron scattering measurements [12] on polycrystalline powders of $Bi_2Fe_4O_9$ were taken using the Merlin [13] and MAPS [14] time-of-flight (ToF) spectrometers at the ISIS facility, UK. The 20 g powder sample was synthesized from a solid state reaction in air and checked to be single phased using a Rigaku MiniFlex x-ray diffractometer. Merlin was operated in rep-rate multiplication mode with the gadolinium Fermi chopper running at 600 Hz and focused incident energies of 120 and 180 meV. On MAPS we used $E_i = 300$ meV with the "sloppy" chopper running at 600 Hz. Finally, inelastic neutron scattering measurements [15] on polycrystalline powders of $Bi_4Fe_5O_{13}F$ were performed on the IN4 [16] ToF spectrometer at ILL, France. The 6.4 g powder sample was synthesized by a solid state reaction in evacuated sealed quartz tubes and used previously for diffraction measurements [4,5]. We used incident neutron energies of 150, 66, and 16.6 meV with the Fermi chopper running at 333 Hz for 150 and 66 meV and 200 Hz for 16.6 meV. Additional measurements at higher energies on the same sample was carried out using the MARI spectrometer at ISIS. The IN4 data was processed using the LAMP [17] software with subsequent checks using Mantid [18]. MAPS, Merlin, and MARI data were processed using Mantid. We
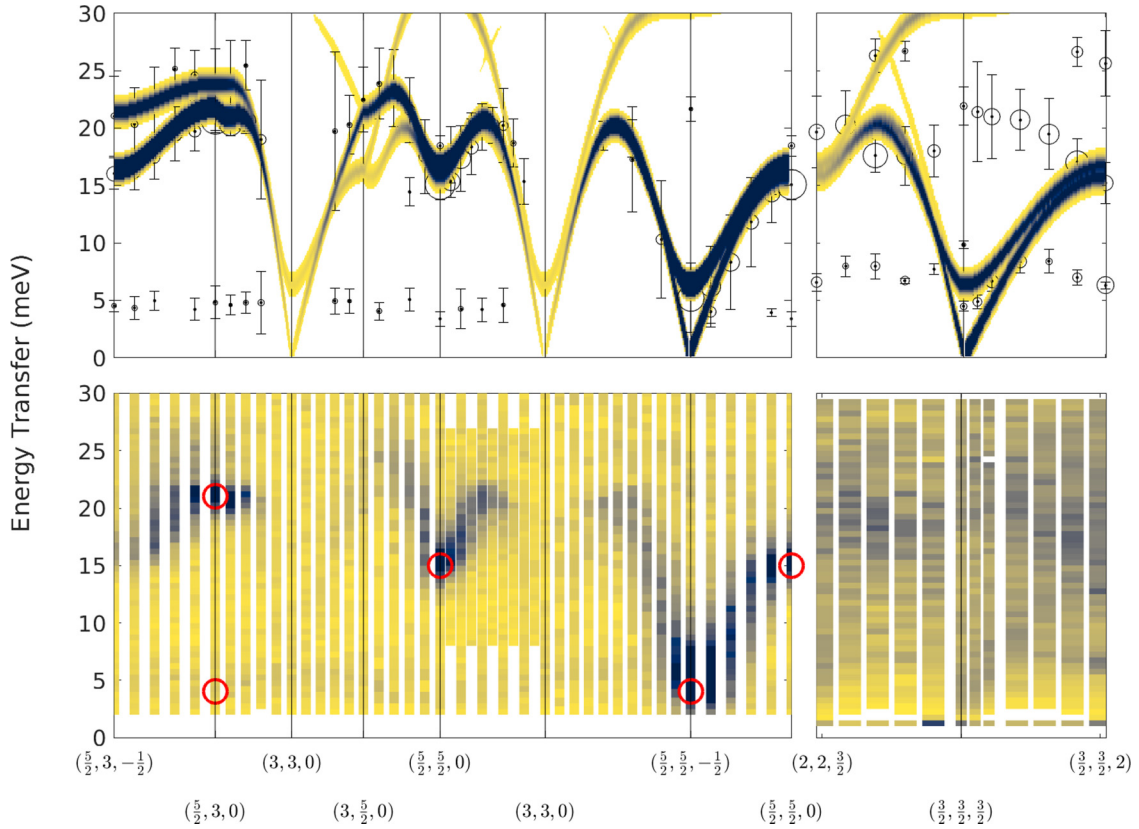
FIG. 2. The magnon dispersion of $Bi_2Fe_4O_9$ at 2 K measured by inelastic neutron scattering on IN20 (bottom left), and calculated from the spin wave model described in the text (top left), together with that measured at 200 K on EIGER (right panels). Markers in the upper panels indicated the fitted peak positions with the marker size proportional to the fitted peak areas, and the error bars proportional to the fitted widths. The color map shows the measured $\chi''(\mathbf{Q}, \omega)$ on an arbitrary scale. The flat mode below 10 meV and that around 20 meV along [00L] in the Eiger data are believed to be phonons, while the other modes are well fitted by the spin wave model. Large red circles indicate the points where polarized neutron measurements were made.

used the SpinW [19,20] and McPhase [21,22] software packages to model the data.

III. INELASTIC NEUTRON SCATTERING

A. $Bi_2Fe_4O_9$

Figure 2 shows the single-crystal unpolarized data for $Bi_2Fe_4O_9$ collected on IN20 (at 2 K) and EIGER (at 200 K). In order to compare the two different temperatures, the measured scattering intensity $S(\mathbf{Q}, \omega)$ was converted to the dynamical susceptibility $\chi''(\mathbf{Q}, \omega)$ via the fluctuation-dissipation theorem $\chi''(\mathbf{Q}, \omega) \propto [1 - \exp(-\beta\hbar\omega)]S(\mathbf{Q}, \omega)$ and it is $\chi''(\mathbf{Q}, \omega)$ which is plotted on an arbitrary scale. The measured dispersion at low temperature is very similar to a recent single crystal inelastic neutron scattering study [23]. Through most of the Brillouin zone, only a single intense dispersive mode was observed in the energy transfer range up to 30 meV. A much weaker, almost flat mode at around 5 meV energy transfer was also seen on both IN20 and Eiger, and another faint dispersive mode between 15 and 25 meV in the [00L] direction is seen in the Eiger data at 200 K but not in the IN20 data. These modes are not well described by linear spin wave theory (see Sec. IV), and are likely to be scattering from phonons. Another possibility which applies only to the higher energy modes is that they could arise from a spurious signal

due to higher order scattering from the monochromator and analyzer. This "$2k_i = 3k_f$ spurion" comes from the second order scattering of neutrons from the monochromator which matches the energy for third order scattering from the analyzer and appears as an apparent inelastic band at an energy transfer of $\frac{5}{4}$ of E_f, which in our case corresponds to 18.4 meV. This would only apply to the EIGER experiments where PG(002) was used for both the analyzer and monochromator. For the IN20 measurements, a Si(111) monochromator combined with a PG(002) analyzer was used, and since there is almost no half-wavelength contamination with Si(111), the $2k_i$ spurion should be absent on IN20. In any case, such a spurious signal should be dispersionless and not change with $\mathbf{Q}$, whereas the signal we observed in the Eiger data does show some dispersion. Thus it is more likely to be a phonon than a spurious signal.

Table I summarizes the longitudinal polarization analysis measurements on IN20 at 2 K at selected reciprocal lattice positions $(\mathbf{Q}, \omega)$. The spectrometer was set to these positions and the cross sections with the neutron beam polarized along the directions $x \| \mathbf{Q}, y \perp \mathbf{Q}$ in the horizontal plane and z vertical was measured in the spin-flip (SF) and non-spin-flip (NSF) channels. We did not perform a rocking scan but left the spectrometer at the fixed $(\mathbf{Q}, \omega)$ for the six measurements per position shown. From these cross sections, signals

TABLE I. Longitudinal polarization analysis measurements at selected zone center and zone boundary positions. All values are counts per 4×10^6 monitor counts (approximately 10 min), except for the measurement at $(\frac{5}{2}30)$, 4 meV which is in counts per 2×10^7 monitor counts. Numbers in parentheses are standard errors.

$(hkl), \hbar\omega$	I_x^{NSF}	I_x^{SF}	I_y^{NSF}	I_y^{SF}	I_z^{NSF}	I_z^{SF}	M_{yy}		M_{zz}	
							NSF	SF	NSF	SF
$(\frac{5}{2}30)$, 4 meV	141	87	142	94	146	93	1(17)	−7(13)	5(17)	−6(13)
$(\frac{5}{2}30)$, 21 meV	41	388	46	347	335	71	5(9)	41(27)	294(19)	317(21)
$(\frac{5}{2}\frac{5}{2}0)$, 15 meV	56	499	73	533	539	71	17(11)	−34(32)	483(24)	428(24)
$(\frac{5}{2}\frac{5}{2}\frac{\bar{1}}{2})$, 4 meV	42	213	43	256	256	33	1(9)	11(20)	214(17)	180(16)

proportional to the spin fluctuations in the y and z directions may be determined using the equations [24]

$$
\begin{aligned}
M_{yy} = \langle M_{\perp y} M_{\perp y}^\dagger \rangle_\omega &= \sigma_y^{\mathrm{NSF}} - \sigma_x^{\mathrm{NSF}} \\
&= \sigma_x^{\mathrm{SF}} - \sigma_y^{\mathrm{SF}}, \qquad (1) \\
M_{zz} = \langle M_{\perp z} M_{\perp z}^\dagger \rangle_\omega &= \sigma_z^{\mathrm{NSF}} - \sigma_x^{\mathrm{NSF}} \\
&= \sigma_x^{\mathrm{SF}} - \sigma_z^{\mathrm{SF}},
\end{aligned}
$$

where $M_\perp$ is the component of the magnetic scattering vector perpendicular to **Q** and $\langle \cdots \rangle_\omega$ indicates the time Fourier-transformed thermal average. We have also assumed that the chiral ($\propto \langle \mathbf{M} \times \mathbf{M} \rangle_\omega$) and nuclear-magnetic interference ($\propto \langle N\mathbf{M} \rangle_\omega$, where N is the nuclear scattering amplitude) terms in the cross section are negligible compared to the strong magnetic signal. This means that the incident polarization was always kept the same and only the flipper on the scattered beam was turned on (for SF) or off (for NSF). The measurements in Table I show that the low energy flat mode around 4–5 meV is nonmagnetic, as indicated by the $(\frac{5}{2}30)$, 4 meV point, implying that this mode is most likely a phonon. The polarized measurements also show that the magnetic fluctuations in the zone center and zone boundaries are almost entirely out-of-plane (along $z \| c$), consistent with an easy plane single-ion anisotropy as will be discussed in Sec. IV.

In addition to the data below 30 meV shown in Fig. 2, we had also measured peaks at around 35 meV which appeared dispersive in the IN20 data. However, later analysis showed that this was an experimental artifact, arising from the inelastic incoherent scattering of a sample Bragg peak from the analyzer. Preliminary spin wave theory calculations based on exchange parameters previously calculated by density functional theory (DFT) [5,25] showed two bands of excitations, with the lower energy band associated with the interlayer exchange interaction and the upper coming from the in-plane interactions. As we had apparently seen both bands in scans on IN20 up to 40 meV, we did not extend the measurements to higher energies at the time. When subsequent analysis indicated that the upper mode is actually spurious scattering, we performed additional high energy measurements on powder samples.

Figures 3 and 4 show the data on $\mathrm{Bi_2Fe_4O_9}$ powder measured on MAPS and Merlin. Additional scattering which follows the magnetic form factor was observed at ≈ 40 meV and between 60 and 80 meV. Modeling the data, we found that the relatively narrow flat mode at 40 meV is associated with the in-phase precession of the ferromagnetically coupled
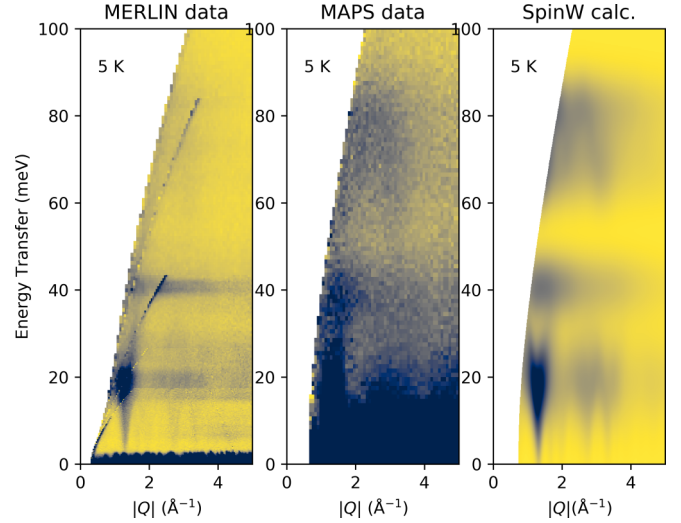

FIG. 3. Powder inelastic neutron scattering data on $\mathrm{Bi_2Fe_4O_9}$ from MERLIN and MAPS at 5 K. Data from multiple MERLIN runs with $E_i = 25$, 38, 62, 120, and 180 meV is shown overlapped on the left panel. MAPS data shows the $E_i = 300$ meV run. Several magnon bands up to 90 meV are visible as described in the text.
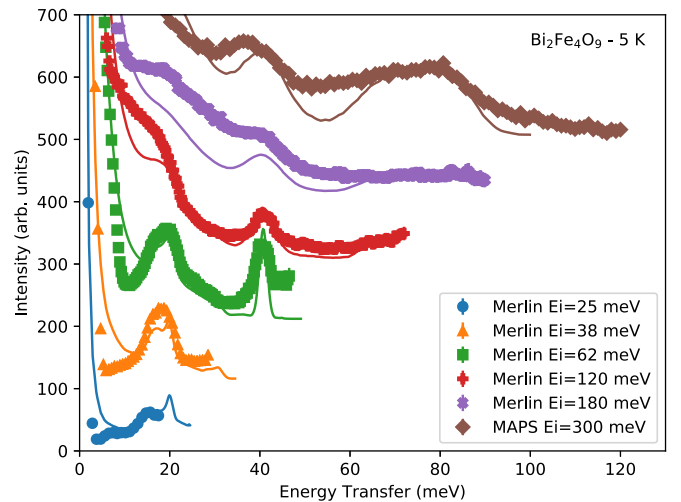

FIG. 4. Cuts along energy transfer of the powder inelastic neutron scattering data on $\mathrm{Bi_2Fe_4O_9}$ from MERLIN and MAPS at 5 K, integrating over the low $|Q|$ region up to 3 Å^{-1}. Solid lines are fits to a spin wave model described in the text.
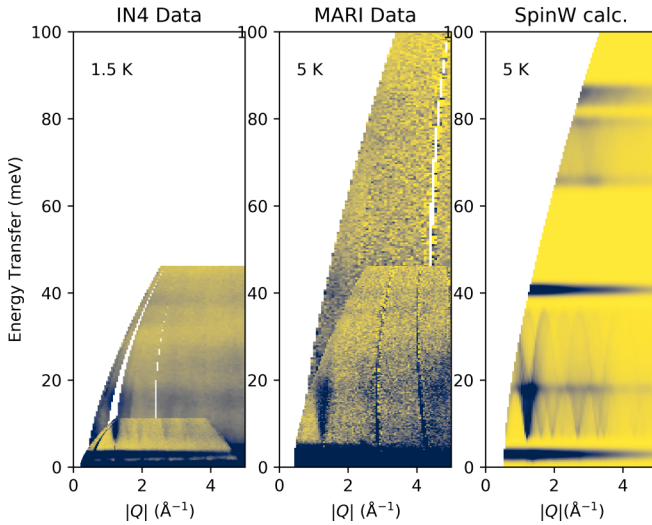
FIG. 5. Powder inelastic neutron scattering data on $Bi_4Fe_5O_{13}F$ from IN4 and MARI at low temperatures. Data from multiple runs with $E_i = 16.6$ and 66 meV from IN4 and $E_i = 66$ and 160 meV from MARI is shown overlapped. Several magnon bands up to 90 meV similar to $Bi_2Fe_4O_9$ are observed as described in the text.

spins which form the fourfold Fe^4 site in the Cairo lattice. The energy of this mode thus serves to pin down the J_{44} exchange parameter which couples these spins. The in-plane dimer interaction J_{33} on the other hand determines the energy separation between the lower and upper magnon bands. That we observed the upper band at relatively high energies (between 60 and 80 meV) thus implies a large $|J_{33}|$ which is significantly larger than anticipated by DFT calculations. Finally, the bandwidths of the magnon bands are determined by the other in-plane interactions (both upper and lower bands) and the interlayer coupling J_c (lower band only).

B. $Bi_4Fe_5O_{13}F$

Figures 5 and 6 show the inelastic neutron spectrum of powder $Bi_4Fe_5O_{13}F$ as 2D contour maps and energy cuts, respectively. Magnetic excitations are seen up to ≈ 80 meV like in $Bi_2Fe_4O_9$. Similarly, the pattern of a strongly dispersive band below 20 meV, a flat band around 40 meV, and another band at higher energies is also seen. The largest difference between the spectra of the two materials is an intense flat mode below the dispersive mode at ≈ 3 meV. This low energy mode is observed only at low temperatures in phase I, and disappears above the $T_1 = 62$ K transition, as shown in Fig. 7. It is thus associated with ordering of the intermediate Fe^{int} layer, which is supported by spin wave modeling where the mode disappears if the moments on the Fe^{int} site is disordered.

In addition, the 40 meV flat band in $Bi_2Fe_4O_9$ appears to be split into two bands in $Bi_4Fe_5O_{13}F$. Like in $Bi_2Fe_4O_9$, this mode is associated with the ferromagnetically coupled fourfold symmetric sites Fe^4. In addition, these ions are coupled to the intermediate layer Fe^{int} sites by the interlayer J_c interaction. However, this antiferromagnetic interaction is not enough to lead to a splitting of the 40 meV band. As explained in the next section, this splitting could be described in spin wave theory only if the intermediate layer Fe^{int} spins are
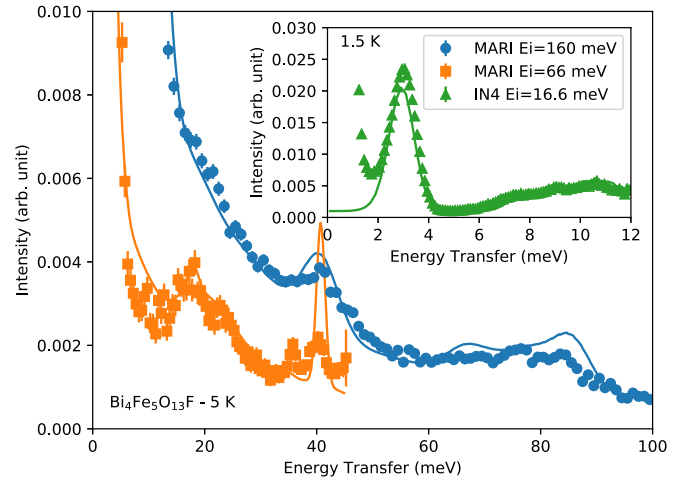

FIG. 6. Cuts along energy transfer of the powder inelastic neutron scattering data on $Bi_4Fe_5O_{13}F$ from IN4 and MARI at low temperatures, integrating over a narrow region around the first magnetic Brillouin zone center. Solid lines are spin wave model fits.

canted with respect to the Fe^4 spins. Since neutron diffraction measurements show that this is not the case, we have been unable to model this splitting in the data.

IV. SPIN WAVE THEORY

The exchange interaction topology for the two materials is shown in Fig. 8. We found that a Heisenberg spin Hamiltonian with isotropic exchange interaction and single-ion anisotropy is enough to model the measured excitations,

$$\mathcal{H} = \sum_{ij} J_{ij}\mathbf{S}_i \cdot \mathbf{S}_j + \sum_i A_i S_z^2(i), \qquad (2)$$
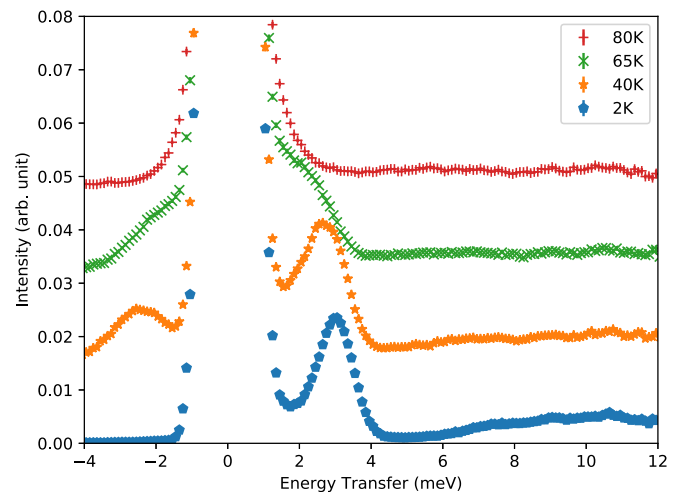

FIG. 7. Temperature dependence of the scattering around the first Brillouin zone center as a function of temperature, as measured on IN4 with $E_i = 16.6$ meV. The mode at ≈ 3 meV is associated with the intermediate layer spins which become disordered above $T_1 = 62$ K: it is clearly present in the low temperature phase below T_1, becomes quasielastic in the intermediate phase between T_1 and $T_2 = 71$ K, and disappears above T_2.
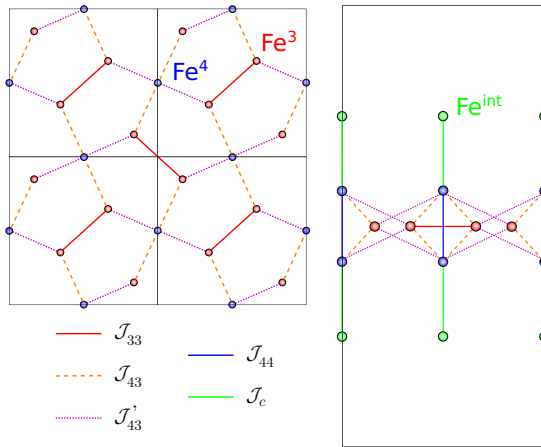
FIG. 8. Exchange couplings between Fe^{3+} spins in the Cairo lattice compounds. Blue circles indicate the fourfold sites Fe^4, red circles are the threefold sites Fe^3, and green circles are the intermediate layer Fe^{int} sites in $Bi_4Fe_5O_{13}F$. In $Bi_2Fe_4O_9$ there are no Fe^{int} sites, and instead the J_c couplings link Fe^4 sites on adjacent pentagon layers.

where positive $J > 0$ indicates antiferromagnetic interactions and positive $A > 0$ indicates an easy-plane single-ion anisotropy (SIA).

Following *ab initio* calculations [5] which indicated that there are preferred easy axes for each spin site within the *a-b* plane, we have also modeled the case where $A < 0$ is negative where the spins prefer to lie parallel or antiparallel to an easy-axis direction along the bond between threefold and fourfold sites. However, the modeling shows that both axial and planar anisotropy scenarios can give almost the same dispersion and intensities (including polarized cross sections at the measured zone center and zone boundary points) albeit with different values of $|A|$.

The exception to this is at low energies close to the zone center or zone boundary, where in the easy-plane case the acoustic magnon is split into two modes. One mode (involving precession out of the plane) is gapped, while the other modes (where the spins only precess within the plane) remains gapless. In the easy-axis case, there is only a single gapped acoustic mode since any precession away from the preferred direction costs energy. However, due to the presence of the magnetic Bragg peak and the incoherent elastic line it is hard to discern the presence of one or two modes. The measured linewidths of the constant-Q scans is quite broad (FWHM ≈ 6 meV, compared to an instrumental resolution of ≈ 1.5 meV) and could be fitted by two peaks but there is no distinct minimum between them. Polarized measurements at the zone boundary acoustic modes [e.g., (330) 4 meV] would have been conclusive but the weak signal and lack of time meant we could not do this. If the anisotropy is planar, this measurement would show that the magnetic fluctuations are polarized in the *a-b* plane, while if the anisotropy is axial, the polarized measurement would show fluctuations to be mainly out-of-plane.

Since our data cannot distinguish between the easy-plane and easy-axis models, we have chosen to use a spin wave model with a single *easy-plane* anisotropy term for $Bi_2Fe_4O_9$

for all sites for simplicity in the following analysis. In the case of $Bi_4Fe_5O_{13}F$, the DFT calculations show that the magnitude of the SIA on the intermediate Fe^{int} sites is much larger than on the others. We have thus modeled this with two easy-plane SIA terms, one for sites in the Cairo-lattice plane and one for the intermediate layer sites.

In terms of the exchange interactions, the real systems $Bi_2Fe_4O_9$ and $Bi_4Fe_5O_{13}F$ deviate from the ideal Cairo pentagonal lattice in several respects. First, the fourfold site is occupied not by a single Fe^{3+} spin, but rather by a pair of spins (each denoted Fe^4 in Fig. 1(b) and Fig. 8) offset above and below the pentagonal plane. This leads additionally to an exchange interaction J_{44} between these spins. Second, due to an asymmetry in the positions of the oxygen ligands, there are two different $\mathcal{J}_{43}$ interactions connecting the fourfold sites and the threefold sites, denoted J_{43} and J'_{43}. Finally, there is a finite interlayer interaction J_c through the fourfold sites. In $Bi_4Fe_5O_{13}F$ this interaction connects the fourfold sites above and below the pentagonal plane with an intermediate layer of Fe^{3+} spins, denoted Fe^{int} in Fig. 8. The threefold sites are denoted Fe^3. We use this notation to ensure a uniform description of the different sites in the physical compounds and the theoretical Cairo lattice, and to reconcile the different notations in the literature for $Bi_2Fe_4O_9$ and $Bi_4Fe_5O_{13}F$ [26].

As noted in the previous section, the in-plane Cairo dimer interaction J_{33} splits the dispersive modes into two bands. The upper band involves mostly precession of the spins on the threefold sites. These spins are antiferromagnetically aligned, so that as J_{33} becomes larger in the positive sense (becomes more antiferromagnetic), this configuration is increasingly stabilized so that it costs more energy to cause the spins to precess away from rigid anti-alignment. Our observation that the upper bands are between 60 and 80 meV thus points to a surprisingly large antiferromagnetic J_{33}, in agreement with [23].

The out-of-phase precession of the ferromagnetically aligned pair of spins above and below the Cairo fourfold site yields a flat band at intermediate energy. A larger ferromagnetic (more negative) J_{44} exchange between these spins will cost this out-of-phase motion more energy and hence push the mode up in energy, while more antiferromagnetic J_{44} will push it down in energy. We observed a flat mode at around 40 meV which points to a moderate *ferromagnetic* J_{44} in contrast with DFT calculations. It is also counter to the findings of Beauvois *et al.* [23] because they posit the flat band to be at ≈ 19 meV and so deduced a moderate *antiferromagnetic* J_{44}. However, 19 meV is very close to an energy transfer of 18.4 meV, which corresponds to a well-known (so-called "$2k_i = 3k_f$") spurion of a triple-axis spectrometer operating with a final wave vector of $k_f = 2.662$ Å^{-1}, as was the case in [23]. We note that we also observe scattering at around this energy in our EIGER data which does not fit the spin wave model and may also be due to this same spurion.

In $Bi_4Fe_5O_{13}F$ at low temperatures we apparently observe at least *two* flat bands around 40 meV, as shown in Figs. 5 and 6. If these bands are magnetic, they may only be explained in terms of spin wave theory by a canting of the intermediate site Fe^{int} spins with respects to the fourfold site Fe^4 spins. This would only arise if there is a very strong easy-axis single-ion anisotropy which would dominate over the exchange

TABLE II. Spin wave exchange parameters fitted to data in meV. Positive values indicate antiferromagnetic exchange. A denotes the single-ion anisotropy term on the threefold and fourfold sites of the Cairo plane, while A' is the term which applies to the intermediate layer spins in $Bi_4Fe_5O_{13}F$ only.

| | $Bi_2Fe_4O_9$ | | |
	This work	Ref. [23]	$Bi_4Fe_5O_{13}F$
J_{33}	27.6(6)	24.0(8)	29(2)
J_{43}	3.1(2)	2.9(1)	4.1(3)
J'_{43}	6.5(2)	6.3(2)	6.4(1)
J_{44}	−0.22(3)	3.7(2)	−0.3(1)
J_c	1.39(5)	1.3(1)	0.49(5)
A	0.096(5)		0.04(2)
A'			0.3(1)

interaction J_c between these spins which tends to keep them in (anti-)alignment. We calculated that A should be an order of magnitude larger than J_c for this to pertain, which seems physically unlikely, given that the Fe^{3+} ion has an $L = 0$ ground state. Moreover, neutron diffraction [5] measurements find that these spins (on sites Fe^4 and Fe^{int}) are antiparallel in phase I at low temperature, with no canting. There are also several optic phonon modes at these energies, but it is hard to discern if any of these modes are magnetic or phononic, because all modes show an initial decrease in intensity from 1 to $4\,Å^{-1}$ followed by an increase in intensity above $6\,Å^{-1}$. Because of the unlikelihood of a large easy-axis single-ion anisotropy and since it would yield a magnetic structure contrary to that observed experimentally, we have chosen the model with modest SIA which yields only a single flat mode.

Also in $Bi_4Fe_5O_{13}F$ there is a low energy flat mode at ≈ 3 meV which is due to precession of the intermediate layer Fe^{int} spins. The energy of this mode depends on J_c and the SIA on the Fe^{int} spins A', while J_c also affects the lower magnon band between 6–25 meV. We found that to fit both these features required a relatively large $A' = 0.3$ meV compared to the value in $Bi_2Fe_4O_9$ of $A' = 0.096$ meV, which is itself surprising for Fe^{3+} which has a $L = 0$ ground state and is needed to explain the ≈ 5 meV anisotropy gap in $Bi_2Fe_4O_9$. However, the large value of A' compared to A is consistent with DFT calculations of the SIA in $Bi_4Fe_5O_{13}F$ [5] which found that the magnitude of SIA on the Fe^{int} site is over 5 times that on the other sites.

Finally, the bandwidths of the lower and upper bands are determined by J_{43} and J'_{43}, while the lower bands are additionally modulated by J_c, since the upper bands involve mostly the threefold sites which are not coupled by J_c.

Taking these considerations into account together with the observed energies of the different magnon bands in the two compounds, we were able to obtain suitable starting parameters for a local minimum simplex search. The fitted exchange interactions are given in Table II. Neutron data files, spin wave models, and data analysis scripts may be obtained from [27].

V. HIGH FIELD MAGNETIZATION

Figure 9 shows the high field magnetization measured in a pulsed field and corresponding mean-field calculations.
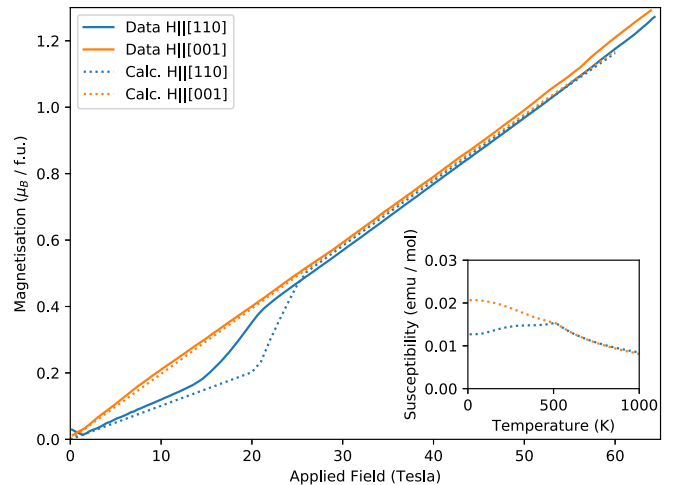

FIG. 9. High-field magnetization of $Bi_2Fe_4O_9$ measured in a pulse field parallel to the [110] and [001] directions (solid lines) and corresponding mean-field calculations (dotted lines). The calculated curves have been scaled to the measured ordered moment of $Bi_2Fe_4O_9$. The inset shows the calculated susceptibility at a field of 0.1 T. A spin-flop transition is observed at ≈ 18 T in the data. In the model this critical field depends on the single-ion anisotropy. The SIA determined from a point charge model (see text) yields a critical field slightly higher than the observation but is qualitatively similar. The slight upturn in the data curve for $H||[110]$ at low fields is a measurement artifact.

A metamagnetic transition is observed around 18 T, and the mean-field calculations reveal it to be a spin-flop transition where the spins cant out of the a-b plane in order to minimize the Zeeman energy of the in-plane field. The critical field depends primarily on the single-ion anisotropy which keeps the spins within the a-b plane, and to a lesser extent on the exchange interactions which prefers the orthogonal Cairo magnetic structure.

The mean-field calculations used the exchange parameters fitted from the INS data as described above, but instead of a simple easy plane anisotropy term, a point charge model was used to calculate the full crystalline electric field. This is needed to use the *intermediate coupling* scheme which includes the effect of the on-site Coulomb and spin-orbit interactions, which we deemed to be more accurate than a simple spin-only approach. We used the nominal charges ($+3|e|$ for Bi and Fe and $-2|e|$ for O) and calculated the effect of these charges on the magnetic $3d$ electrons of the Fe sites by including contributions from neighboring charges up to 6.5 Å from a given Fe site, which covers up to second neighboring Fe ions. These calculations found that the crystal field splitting on the threefold and fourfold sites had similar magnitude, yielding an overall splitting of ≈ 0.4 meV. This would correspond to a planar SIA term of $A_{pc} = 0.06$ meV, which is 60% of the value found from fitting the spin anisotropy gap. Scaling up the magnitude of the crystal field splitting to match the measured spin anisotropy gap would increase the spin-flop transition field by an equivalent amount. Nonetheless, the chosen point charge model still overestimates the critical field of the spin-flop transition, by $\approx 20\%$.

In any case, the point charge calculations showed that additional anisotropy is present in the *ab* plane, with the threefold sites preferring to align at 52° to the *a* axis, and at 90°, 180°, and 270° to this angle. The fourfold sites, on the other hand, preferred to align parallel and antiparallel to *c* but are kept pinned to the *a-b* plane by the exchange coupling with the threefold sites. This is in contrast to the DFT calculations which found that all the moments preferred to lie within the *a-b* plane. We should note here that the point charge model is quite a coarse model and does not include many effects such as charge transfer and covalency which the DFT calculation does take into account.

In addition, in order to match the measured slope of the magnetization, we found that we needed to scale the mean-field calculations (which assumed a full ordered moment of 5 μ_B/Fe) by the ordered moment obtained by neutron diffraction measurements [3], ≈ 3.5 μ_B. The scaled magnetization is shown in Fig. 9. We also calculated the temperature dependence of the magnetization in a 0.1 T field, shown as an inset to Fig. 9. Because of the large J_{33} interaction between pairs of threefold symmetric spins, we have used a cluster mean-field method to calculate $M(T)$. In the calculation, the pairs joined by J_{33} are treated as a cluster using exact diagonalization, but other interactions are treated in the mean-field approximation. This reduces the calculated T_N compared with a pure mean-field calculation but still retains some effects of J_{33}. The results agrees qualitatively with the measurements of Ressouche *et al.* [3] but overestimates the ordering temperature by a factor of 2, yielding $T_N^{cmf} = 510$ K. In contrast, a pure mean-field calculation gives $T_N^{cmf} = 1150$ K.

Finally, we also applied the point charge calculations to $Bi_4Fe_5O_{13}F$, and found again that the fourfold sites preferred to orient along *c*, while the threefold sites preferred an in-plane direction offset 22° to the *a* axis, and the intermediate layers to align along the $\langle 110 \rangle$ directions.

VI. DISCUSSIONS

In agreement with previous INS measurements [23], we find a very strong dimer interaction J_{33} between the three-fold symmetric sites of the Cairo lattice in both $Bi_2Fe_4O_9$ and $Bi_4Fe_5O_{13}F$, which puts these materials firmly within the *orthogonal* phase of the theoretical phase diagram. In both compounds the values of J_{33} deduced from the spin wave spectra is almost three times that calculated from DFT [4,5], while the deduced value of the other exchange interactions are of comparable magnitudes to the theoretical value. The large J_{33} also pushes the calculated mean-field ordering temperature to above 1000 K, but goes some way to explaining the large Curie-Weiss temperature $\theta_{CW} \approx -1670$ K (the sum of the deduced exchanges for $Bi_2Fe_4O_9$ is -1585 K). We thus also used a cluster mean-field method that treats the dimer linked by J_{33} as a cluster and applies exact diagonalization to this cluster, which is then coupled to the other spins in a mean-field fashion. This calculation reduces the calculated $T_N^{cmf} = 510$ K which is still over twice the measured $T_N = 245$ K. Given the large J_{33}, one would expect the dimers to still be strongly coupled well above the overall ordering temperature T_N. As noted by Beauvois *et al.* [23], this would lead to a correlated paramagnetic state which could give rise to novel phenomena.

The deduced exchange parameters for $Bi_2Fe_4O_9$ and $Bi_4Fe_5O_{13}F$ are quite similar, with the main difference being the deduced interlayer coupling, which was found to be $J_c = 1.39$ meV in $Bi_2Fe_4O_9$ and $J_c = 0.49$ meV in $Bi_4Fe_5O_{13}F$. This could perhaps explain part of the decrease in ordering temperature from $T_N = 238$ K in $Bi_2Fe_4O_9$ to $T_N = 178$ K in $Bi_4Fe_5O_{13}F$, as the in-plane interactions in $Bi_4Fe_5O_{13}F$ are deduced to be slightly larger than in $Bi_2Fe_4O_9$. $Bi_4Fe_5O_{13}F$ should thus also show the same correlated paramagnetic behavior as $Bi_2Fe_4O_9$, but at a slightly lower temperature.

Finally, in contrast to the expectation of the $L = 0$ ground state of the Fe^{3+} ion, we found that there is a non-negligible single-ion anisotropy in both $Bi_2Fe_4O_9$ and $Bi_4Fe_5O_{13}F$. This manifests in $Bi_2Fe_4O_9$ in a spin anisotropy gap of ≈ 5 meV and a spin-flop transition at a critical field of ≈ 17 T. The gap is not directly measurable in $Bi_4Fe_5O_{13}F$ because of the low energy flat mode at ≈ 3 meV due to precession of intermediate layer spins in the lowest temperature ordered phase. However, fitting the energy of this mode yields an even higher SIA than for $Bi_2Fe_4O_9$, which reflects the more distorted octahedral environment of the Fe^{int} spins, and is in agreement with the larger SIA found for these sites by DFT calculations [5]. This gives support to the model of Tsirlin *et al.* [5] for the SIA being the origin of the series of phase transitions in $Bi_4Fe_5O_{13}F$.

In this model the weak interlayer couplings means that the intermediate layer Fe^{int} spins are more susceptible to thermal fluctuations and become disordered first, at $T_1 = 62$ K. Below this temperature, the large SIA on these Fe^{int} spins combined with the J_c coupling constrains the Fe^4 spins to be antiparallel to the Fe^{int} spins. The intralayer interactions then favors a orthogonal magnetic structure with a particular mutual arrangement of adjacent Fe^4 spins described by a local vector chirality introduced in Ref. [5]. However, the intrinsic SIA of the Fe^3 and Fe^4 sites prefers a different arrangement of the Fe^4 spins described by the opposite sign of the local vector chirality, which is stabilized at high temperatures when the Fe^{int} spins become disordered, in the phase between $T_2 = 71$ K and $T_N = 178$ K. In between is a phase where the direction of preferred orientations of the Fe^4 spins determined by the competing SIA and intralayer interactions crosses over giving a collinear, partial-ordered structure in the narrow temperature window between $T_1 = 62$ K and $T_2 = 71$ K. Although this collinear structure is very similar to the theoretically predicted structure in the limit of small $\mathcal{J}_{43}/\mathcal{J}_{33}$ [2], it does not have the same origin. In the theory of Rousochatzakis *et al.* [2], which is based on a Heisenberg Hamiltonian without single-ion anisotropy, the collinear phase is driven by quantum fluctuations. Whereas in the model of Tsirlin *et al.* [5] it is a crossover between two orthogonal ordered phases with opposite local vector chiralities, necessitating a collinear state in between. Because we have a high spin ($S = 5/2$) system, the threshold for the quantum fluctuations driven model is $\mathcal{J}_{43}/\mathcal{J}_{33} \lesssim 0.1$ [5]. Our larger value for J_{33} than the DFT calculated values used by Tsirlin *et al.* [5] suggests that we are approaching this limit in this case ($\mathcal{J}_{43}/\mathcal{J}_{33} = 0.11$ and $J'_{43}/\mathcal{J}_{33} = 0.24$). However, the experimental evidence for a relatively large single-ion anisotropy and the fact that the collinear phase exists only in a narrow range of temperature between two orthogonal phases indicates that the single-ion

anisotropy driven model for the origin of this phase is correct for $Bi_4Fe_5O_{13}F$. This also suggests that there is scope for further theoretical work to extend the phase diagram to include a single-ion anisotropy term, in order to better account for the behavior of the materials which realize the Cairo lattice.

[1] C. Lacroix, P. Mendels, and F. Mila, *Introduction to Frustrated Magnetism: Materials, Experiments, Theory* (Springer, Berlin, 2011).

[2] I. Rousochatzakis, A. M. Läuchli, and R. Moessner, Phys. Rev. B **85**, 104415 (2012).

[3] E. Ressouche, V. Simonet, B. Canals, M. Gospodinov, and V. Skumryev, Phys. Rev. Lett. **103**, 267204 (2009).

[4] A. M. Abakumov, D. Batuk, A. A. Tsirlin, C. Prescher, L. Dubrovinsky, D. V. Sheptyakov, W. Schnelle, J. Hadermann, and G. Van Tendeloo, Phys. Rev. B **87**, 024423 (2013).

[5] A. A. Tsirlin, I. Rousochatzakis, D. Filimonov, D. Batuk, M. Frontzek, and A. M. Abakumov, Phys. Rev. B **96**, 094420 (2017).

[6] J. Oh, M. D. Le, J. Jeong, J.-h. Lee, H. Woo, W.-Y. Song, T. G. Perring, W. J. L. Buyers, S.-W. Cheong, and J.-G. Park, Phys. Rev. Lett. **111**, 257202 (2013).

[7] J. Oh, M. D. Le, H.-H. Nahm, H. Sim, J. Jeong, T. G. Perring, H. Woo, K. Nakajima, S. Ohira-Kawamura, Z. Yamani, Y. Yoshida, H. Eisaki, S.-W. Cheong, A. L. Chernyshev, and J.-G. Park, Nat. Commun. **7**, 13146 (2016).

[8] U. Stuhr, B. Roessli, S. Gvasaliya, H. Rønnow, U. Filges, D. Graf, A. Bollhalder, D. Hohl, R. Bürge, M. Schild, L. Holitzner, C. Kaegi, P. Keller, and T. Mühlebach, Nucl. Instrum. Methods Phys. Res. A **853**, 16 (2017).

[9] J. Kulda, J. Šaroun, P. Courtois, M. Enderle, M. Thomas, and P. Flores, Appl. Phys. A **74**, s246 (2002).

[10] S. A. Kim, C.-H. Lee, M.-K. Moon, S.-J. Cho, T.-S. Yoon, Y. Noda, and Y. Ishikawa, Neutron News **24**, 33 (2013).

[11] M. D. Le, M. Enderle, A. Tsirlin, and E. Wheeler, Determination of the exchange parameters in the frustrated cairo pentagon lattice compound $Bi_2Fe_4O_9$, doi:10.5291/ILL-DATA.4-01-1428 (2015).

[12] M. D. Le, Magnetic excitations in a frustrated cairo pentagon lattice, doi:10.5286/ISIS.E.RB1820598 (2018).

[13] R. I. Bewley, T. Guidi, and S. Bennington, Notiziario Neutroni Luce Sincrotrone **14**, 22 (2009).

[14] R. A. Ewings, J. R. Stewart, T. G. Perring, R. I. Bewley, M. D. Le, D. Raspino, D. E. Pooley, G. Škoro, S. P. Waller, D. Zacek, C. A. Smith, and R. C. Riehl-Shaw, Rev. Sci. Instrum. **90**, 035110 (2019).

[15] M. D. Le, B. Fåk, A. Tsirlin, and E. Wheeler, Magnetic excitations in the frustrated Cairo pentagon lattice compound $Bi_4Fe_5O_{13}F$, doi:10.5291/ILL-DATA.4-01-1427 (2015).

[16] G. Cicognani, H. Mutka, and F. Sacchetti, Phys. B: Condens. Matter **276-278**, 83 (2000).

[17] D. Richard, M. Ferrand, and G. Kearley, J. Neutron Res. **4**, 33 (1996).

[18] O. Arnold, J. Bilheux, J. Borreguero, A. Buts, S. Campbell, L. Chapon, M. Doucet, N. Draper, R. F. Leal, M. Gigg, V. Lynch, A. Markvardsen, D. Mikkelson, R. Mikkelson, R. Miller, K. Palmen, P. Parker, G. Passos, T. Perring, P. Peterson, S. Ren, M. Reuter, A. Savici, J. Taylor, R. Taylor, R. Tolchenov, W. Zhou, and J. Zikovsky, Nucl. Instrum. Methods Phys. Res. A **764**, 156 (2014).

[19] S. Toth and B. Lake, J. Phys.: Condens. Matter **27**, 166002 (2015).

[20] S. Tóth *et al.*, http://www.spinw.org.

[21] M. Rotter, M. D. Le, A. T. Boothroyd, and J. A. Blanco, J. Phys.: Condens. Matter **24**, 213201 (2012).

[22] M. Rotter *et al.*, http://www.mcphase.de.

[23] K. Beauvois, V. Simonet, S. Petit, J. Robert, F. Bourdarot, M. Gospodinov, A. A. Mukhin, R. Ballou, V. Skumryev, and E. Ressouche, Phys. Rev. Lett. **124**, 127202 (2020).

[24] M. Enderle, Collection SFN **13**, 01002 (2014).

[25] Z. V. Pchelkina and S. V. Streltsov, Phys. Rev. B **88**, 054424 (2013).

[26] In the literature for $Bi_2Fe_4O_9$, Fe_1 is used for the threefold sites we label Fe^3 and Fe_2 for the sites we label Fe^4 [3,23]. In contrast, the literature for $Bi_4Fe_5O_{13}F$ uses Fe_1 for the *fourfold* site Fe^4, Fe_2 for the threefold site Fe^3, and Fe_3 for the intermediate layer site Fe^{int} [5].

[27] M. D. Le *et al.*, http://github.com/mducle/cairo-data.